OPEN ACCESS
IOP PUBLISHING
Made open access 2 April 2013
CLASSICAL AND QUANTUM GRAVITY
Class. Quantum Grav. **30** (2013) 035004 (20pp)
doi:10.1088/0264-9381/30/3/035004

# Experimental test of higher-order Laguerre–Gauss modes in the 10 m Glasgow prototype interferometer

**B Sorazu[1], P J Fulda[2], B W Barr[1], A S Bell[1], C Bond[2], L Carbone[2], A Freise[2], S Hild[1], S H Huttner[1], J Macarthur[1] and K A Strain[1]**

[1] SUPA School of Physics and Astronomy, University of Glasgow, Glasgow G12 8QQ, Scotland, UK
[2] School of Physics and Astronomy, University of Birmingham, Birmingham B15 2TT, UK

E-mail: borja.sorazu@glasgow.ac.uk

Received 8 November 2012, in final form 11 December 2012
Published 11 January 2013
Online at stacks.iop.org/CQG/30/035004

**Abstract**

Brownian noise of dielectric mirror coatings is expected to be one of the limiting noise sources, at the peak sensitivity, of next generation ground based interferometric gravitational wave (GW) detectors. The use of higher-order Laguerre–Gauss (LG) beams has been suggested to reduce the effect of coating thermal noise in future generations of gravitational wave detectors. In this paper we describe the first test of interferometry with higher-order LG beams in an environment similar to a full-scale gravitational wave detector. We compare the interferometric performance of higher-order LG modes and the fundamental mode beams, injected into a 10 m long suspended cavity that features a finesse of 612, a value chosen to be typical of future gravitational wave detectors. We found that the expected mode degeneracy of the injected $LG_{3,3}$ beam was resolved into a multiple peak structure, and that the cavity length control signal featured several nearby zero crossings. The break up of the mode degeneracy is due to an astigmatism (defined as $|R_{cy} - R_{cx}|$) of $5.25 \pm 0.5$ cm on one of our cavity mirrors with a radius of curvature ($R_c$) of 15 m. This observation agrees well with numerical simulations developed with the FINESSE software. We also report on how these higher-order mode beams respond to the misalignment and mode mismatch present in our 10 m cavity. In general we found the $LG_{3,3}$ beam to be considerably more susceptible to astigmatism and mode mismatch than a conventional fundamental mode beam. Therefore the potential application of higher-order Laguerre–Gauss beams in future gravitational wave detectors will impose much more stringent requirements on both mode matching and mirror astigmatism.

PACS numbers: 04.80.Nn, 95.55.Ym, 95.75.Kk, 95.75.Pq

(Some figures may appear in colour only in the online journal)

  

## 1. Introduction

Second generation, or 'advanced' ground based interferometric gravitational wave detectors, such as Advanced LIGO and Advanced VIRGO [1, 2], are currently under construction. These detectors are designed to have peak sensitivity approximately one order of magnitude better than first-generation detectors [3, 4].

Such detectors measure wave amplitude (strains in space), so the sensitivity improvement increases the detection range by the same factor and for uniformly distributed sources the rate should increase by a factor of $10^3$ in proportion to the volume, giving rates of tens or hundreds of events per year [5]. Advanced detectors operating at design sensitivity should not only achieve the first direct gravitational wave detection but they will also open the era of gravitational-wave astronomy.

Advanced detectors are predicted to be limited by several noise sources with varying contributions according to frequency. Filtered seismic noise produces an effective low-frequency cut-off at 10 Hz. Other important sources at low and mid frequencies (below 40 Hz) are radiation pressure noise, suspension thermal noise and gravity gradient noise, all of which decline with frequency. The major noise source whose effect *increases* with frequency such that it always dominates above the frequency of peak sensitivity, near 100 Hz, is shot noise [3].

It is important to maximize peak sensitivity: signals such as compact-object coalescences, sweep across a frequency range, and a large part of the signal is obtained as it sweeps through the frequency range of peak sensitivity. In that frequency range between 40 and 90 Hz, the dominant noise contribution is expected to arise from thermal noise in the mirrors (test-masses) of the interferometer (coating thermal noise). As described by the fluctuation–dissipation theorem, thermal noise originates from every source of dissipation, in systems at finite temperature. In advanced detectors the single most important source of thermal noise is mechanical loss in high-refractive index layers of the alternating-index dielectric mirror coatings [6]. The design of the coatings is tightly constrained by the need to have ultra-low optical loss, leaving limited flexibility to control mechanical loss. The resulting thermal noise appears as random motion of patches, from atomic-scale upwards, of the mirror surface. The interferometer measures the relative displacements between such mirror coatings on the various interferometer mirrors. Thus the detector is sensitive to such noise, particularly in current designs where a relatively compact beam of Gaussian intensity profile is employed. The standard fundamental mode, $\mathrm{TEM}_{0,0}$, laser beam has to be of small dimension to ensure low optical loss due to clipping of the beam at the edge of the mirror.

Approaches under consideration for the reduction of such thermal noise include: cooling the mirrors to cryogenic temperatures [7]; substituting the coating materials with those of lower mechanical loss [8]; and employing light beams in the interferometer with alternative intensity profiles to the fundamental mode shape [9, 10]. The last approach is the subject of this paper. The objective is a more homogeneously distributed intensity pattern, for fixed clipping loss, such that thermal vibrations are more effectively averaged-out over the mirror surface. A generic term for such profiles is *flat beams*—three classes of which have been considered for implementation on gravitational wave detectors: mesa beams [11], optimized conical beams [12] and higher-order LG beams [13]. The last class is the focus of this work and has the advantage of compatibility with normal spherical mirrors which also support Gaussian modes and which are currently used in GW detectors. Spherical mirrors are available with smooth, well-figured surfaces, benefiting from decades of production experience.

Numerical simulations and benchtop experiments have produced positive results showing the potential of higher-order LG modes in interferometric applications [10, 13, 15]. The

simulations show a reduction in coating thermal noise by a factor of ≈1.7 in terms of amplitude spectral density [13]. This earlier work together with the fact that $LG_{3,3}$ modes are included as baseline in the design of ET [16, 17], a third-generation gravitational wave detector, encouraged us to take the next step of testing the technique in an environment similar to a full-scale detector, namely the 10 m gravitational wave interferometer prototype at Glasgow.

In this paper we describe the procedure employed to generate a higher-order LG beam at the 10 m prototype. We present several results: a comparison of the interferometric performance of higher-order LG modes and the fundamental mode in the prototype cavity, a comparison of the longitudinal control signals generated under the same conditions for both mode types, and results of an investigation of the observed effects of higher-order spatial mode pseudo-degeneracy.

## 2. Laguerre–Gauss modes and mode degeneracy

Laguerre–Gauss modes form a complete set of orthogonal functions that can describe the amplitude distribution of any paraxial beam. Their normalized complex amplitude can be expressed, for the helical mode set, in cylindrical polar coordinates $(r, \phi, z)$ around the optical axis as [19]:

$$\mathrm{LG}_{p,l}(r,\phi,z) = \frac{1}{w(z)}\sqrt{\frac{2p!}{\pi(|l|+p)!}}\left(\frac{\sqrt{2}r}{w(z)}\right)^{|l|} L_p^{|l|}\left(\frac{2r^2}{w^2(z)}\right) \times \mathrm{e}^{-\left(\frac{r^2}{w^2(z)}\right)} \cdot \mathrm{e}^{-\mathrm{i}\left[\frac{kr^2}{2R_c(z)} - l\phi - (2p+|l|+1)\Psi(z)\right]}. \quad (1)$$

Here $p$ and $l$ are the radial and azimuthal indices, $k$ is the wavenumber, $R_c(z)$ is the curvature of the phase-front or *radius of curvature* at the position $z$ in the optical axis, $\Psi(z) = \arctan(z\lambda/\pi w_0^2)$ is the Gouy phase, $w(z)$ is the beam radius and $w_0 = w(z=0)$ is the beam waist. Finally, $L_p^{|l|}(x)$ are the associated Laguerre polynomials.

The power distribution of helical LG modes consists of multiple concentric rings with $p+1$ radial nodes (if $l \neq 0$). For instance the $LG_{3,3}$ mode, on which this work concentrates, has four radial nodes as shown in figure 1. The power distribution becomes wider for larger mode indices, and the peak power decreases. Thus for the same mirror diameter, scattering losses and integrated beam power, the multi-ringed power distribution of LG modes is wider and flatter than the distribution of a fundamental mode $TEM_{0,0}$ beam (as shown in figure 2). This is why higher-order LG mode beams provide reduced thermal noise in the measurement, in comparison with the fundamental mode beams.

The complex-exponential term of equation (1) indicates that the phase difference between different LG modes is given by the term $(2p + |l| + 1)\Psi(z)$, of which only the term $2p + |l|$ varies. This quantity is referred to as the *spatial order* of the LG mode. Modes of the same order will acquire the same round-trip phase shift while circulating in a cavity with spherical mirrors and so they cannot be distinguished in the frequency spectrum. The LG modes of the same order are therefore *degenerate* in the cavity. In particular the $LG_{3,3}$ mode would be degenerate with nine other order nine modes: $LG_{0,\pm9}$, $LG_{1,\pm7}$, $LG_{2,\pm5}$, $LG_{3,-3}$ and $LG_{4,\pm1}$).

In practical cavities, with mirror surface distortions that deviate from perfect spheres, the purity of the resonant higher-order mode is affected as the injected beam mode couples into the other nominally-degenerate modes. Gravitational wave detectors rely on excellent matching of optical cavities which form the two arms of the interferometers to achieve rejection of common-mode instrumental noise. As it is probable that the mirror surface distortions would differ between the arms, the mode content would differ and the contrast of the interference of light returning from the two arms would be degraded, spoiling detector sensitivity. For a more

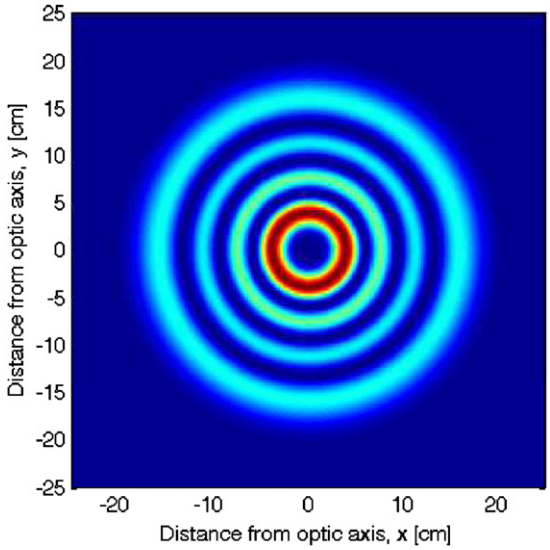


**Figure 1.** Intensity profile of an helical $LG_{3,3}$ mode beam with a beam radius of ≈5.8 cm. The four radial nodes are clearly visible.

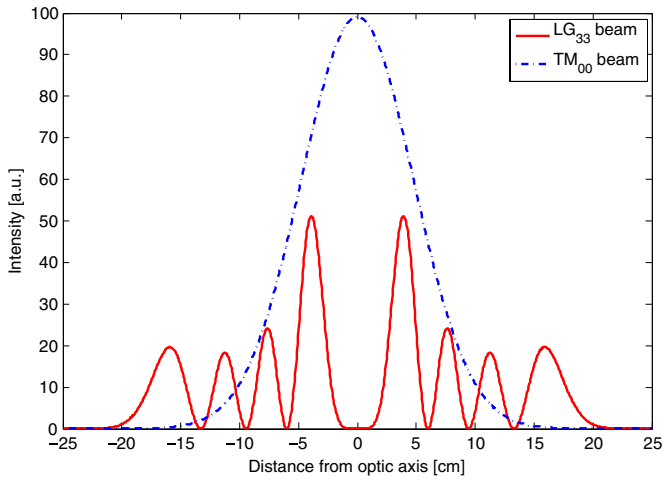


**Figure 2.** Comparison of the intensity profiles of an $LG_{3,3}$ mode (solid line) and the fundamental mode $TEM_{0,0}$ (dashed line) beams. Both profiles have been normalized to have the same integrated power and 1 ppm clipping losses. The radius of the $LG_{3,3}$ mode beam is ≈5.8 cm (same as in figure 1), and for the fundamental mode is ≈ 9.5 cm.

detailed study of higher-order LG mode degeneracy and mode coupling in realistic cavities refer to [21, 20].

Mirror surface distortions break the degeneracy between modes of the same spatial order. The resulting modes will show slightly different resonant frequencies due to the changes in the effective mirror curvature, or cavity length, or both. We will refer to this effect as *mode pseudo-degeneracy* or *frequency splitting*. In order for this effect to be observable the shift in resonant frequency must be larger than the cavity linewidth in order to resolve the resonance peaks of the pseudo-degenerate modes.

LG modes can be described as a sum of Hermite–Gauss (HG) modes as per the decomposition given in [13]. An interesting feature of this transformation of basis is that a given $LG_{p,l}$ mode corresponds to the superposition of $2p + |l| + 1$ $HG_{n,m}$ modes of the order $n + m = 2p + |l|$. HG modes present a grid-like Cartesian symmetry in contrast to the cylindrical symmetry of the LG modes. If a higher order mode is resonant in a cavity lacking perfect cylindrical symmetry (such as an astigmatic cavity), the resonant LG mode content is suppressed in favor of the corresponding HG modes from the decomposition.

## 3. Experimental procedures

### *3.1. The facility*

Our 10 m prototyping facility for gravitational wave detectors is housed in a clean-room suited to handling low-loss optics. The facility was designed to test optical topologies and component sub-systems for advanced interferometry (second generation and beyond) [22–24]. The vacuum infrastructure, the design of suspensions for the interferometer optics, and the control infrastructure are all similar to those of the interferometric gravitational wave detector GEO 600 [25], although with 10 m arms that are folded parallel, rather than 600 m arms that are nearly orthogonal as required for a working detector.

Nine interconnected vacuum tanks are arranged to house a variety of optical configurations. The LG experiment was set up on the optical bench carrying the laser source and injection optics, and one of the nominally 10 m long 'arms' of the vacuum system contained the $9.812 \pm 0.001$ m long Fabry–Perot test cavity. This cavity is formed between two suspended mirrors: an inboard test mass (ITM) and an end test mass (ETM). The cavity length was measured *in situ* by determining the frequency spacing between consecutive fundamental modes scanned using the phase-lock loop (PLL) configuration described below. The measured free spectral range (FSR) was $15.276 \pm 0.001$ MHz.

The type of laser employed is a single-mode, single-frequency, continuous wave Innolight Mephisto Nd:YAG non-planar ring oscillator, operating at up to 2W output.

The ETM is a high quality optic of 2.7 kg mass, with ion-beam sputtered multi-layered dielectric reflective coatings on a fused silica substrate, giving a reflectivity of 99.996% at 1064 nm. This mirror has a nominal radius of curvature $R_c$ of 15 m and a diameter of 12.5 cm although only the central 6 cm diameter area is coated.

The ITM is an *off-the-shelf* 1 inch diameter flat mirror manufactured by CVI Melles Griot to a manufacturer measured reflectivity of 98.98% at 1064 nm. This small mirror was mounted in a supporting aluminium mass, also of about 2.7 kg.

The ITM in its mount, and the ETM are both suspended as the final stages in a triple pendulum, i.e. three vertically-cascaded stages. Alignment and control forces can be applied via coil-magnet actuators acting from mechanically similar reaction pendulums suspended 'behind' the mirrors (i.e. outside the cavity, with holes in the reaction masses to admit light). Active damping was applied in all 6 degrees of freedom of the top stage of each suspension.

The nominal finesse of the 10 m cavity is 612, a value chosen to be typical of the arm cavities in advanced detectors. The half-width half-maximum of the cavity resonance, also known as the linewidth of the cavity, is therefore 12.48 kHz.

### *3.2. Generation of the LG33 beam*

The method of generating the $LG_{3,3}$ mode beam in the Glasgow 10 m prototype was designed to allow the light to be diverted easily to other experiments taking place in the same period. Figure 3 shows the arrangement of the stand-alone $LG_{3,3}$ mode generator, including input

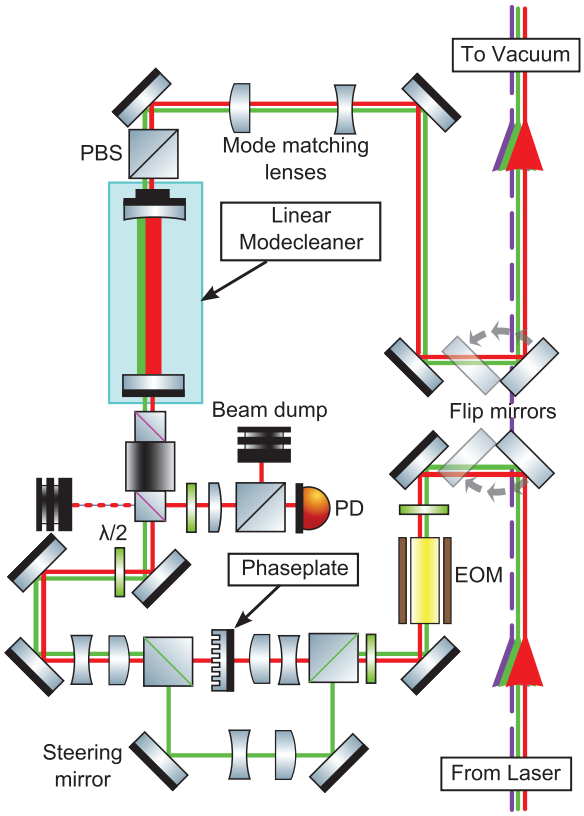


**Figure 3.** The $LG_{3,3}$ mode beam generation optical setup on the input optics bench. The red (or dark color for the printed version of the paper) line shows the $LG_{3,3}$ mode path, the green (or light color) line indicates the fundamental mode path that bypasses the phaseplate, and the purple dashed line represents the original fundamental mode beam path. PBS is a polarizing beamsplitter, EOM is an electro-optic modulator and PD is a photodiode.

and output 'flip' mirrors to divert the existing fundamental mode beam and to re-inject the converted $LG_{3,3}$ mode beam into the original beam path (shown in purple dashed line).

A single-mode, polarization-maintaining optical fiber is employed as a spatial filter to purify the laser mode. The input to the LG generator is taken after the output coupler of this fiber. This beam passes through an electro-optic modulator (EOM) which imposes phase modulation sidebands, at 12 MHz, for the purpose of length control of the downstream linear mode cleaner (LMC) cavity (described below). Next, a polarizing beamsplitter (PBS) allows the input beam to go through (shown in figure 3 in red or dark color for the printed version of the paper) or bypass (shown in figure 3 in green or light color) an etched diffractive phase-plate, similar to that used in [14], that converts the fundamental mode to the desired $LG_{3,3}$ mode. The bypass path allows the propagation of the fundamental mode through the LMC. Since the light transmitted by the mode cleaner arises from a cavity eigenmode, the transmitted fundamental and $LG_{3,3}$ mode beams should, ideally, have the same alignment and mode matching relative to the suspended cavity downstream. We therefore aligned and mode-matched the suspended cavity to the fundamental mode, in the routine manner, before transitioning to the $LG_{3,3}$ mode beam which should then be found to be matched to the cavity. For this purpose, either beam path (red or green, for the printed version it would be dark or light color) can be blocked.

The bypass and LG-mode paths are recombined, at a PBS, before the combined beams are matched to the cavity eigenmode via a telescope. The LMC is 21 cm long, giving it an FSR of 714 MHz. It is a plano-concave cavity with a finesse of 172 and stability ($g$) parameter of $\approx 0.8$. Its main function is to increase the mode purity of the LG beam as demonstrated in [15]. The length of the cavity is controlled, by feedback to a PZT-mounted mirror, to maintain it on resonance for modes of order 9. The signal for this is obtained using the 12 MHz phase modulation sidebands in the Pound–Drever–Hall (PDH) method [18].

The stable transmitted beam is passed through a second telescope that matches it to the beam parameters of the original (purple dashed line) path at the second flip mirror. Although not shown in figure 3, the beam next passes through the injection optics for the 10 m arm cavity. First comes an EOM at 18 MHz, which imposes phase modulation sidebands for PDH locking of the frequency of the laser source to the length of the arm cavity. This can be used to keep either the $LG_{3,3}$ beam or the fundamental mode beam on resonance, depending on which is selected. A Faraday isolator (FI) prevents back-reflections from the arm cavity entering the LMC and laser source and diverts the reflected light to the length sensing photodiode (PD), for PDH sensing. Finally the input beam goes through a mode-matching telescope before reaching the suspended arm cavity (several plane beam-steering mirrors are omitted from this description).

### *3.3. Description of the experimental setup*

To allow comparison of the longitudinal control signals generated by the fundamental and higher-order beams, it is necessary to be able to lock the 10 m arm cavity to the required mode. To investigate mode pseudo-degeneracy it was necessary to be able to measure the mode spectrum. Figure 4 shows the experimental setup implemented to achieve these goals.

Laser #1 is associated with LG mode generation, while laser #2 is available to pump the cavity fundamental mode to provide a stable reference for the mode spectrum measurement. In each case the PDH method is applied to lock the appropriate laser to the cavity. Feedback is applied to the PZT (fast control) and crystal temperature (slow control) inputs provided on the laser.

In the experiment to compare locking with fundamental and higher-order modes, laser #1 was controlled as described above, and laser #2 is not used. In experiments to measure the spectrum of the higher-order cavity modes, the phase-locked-loop (PLL) arrangement provides a method of methodically scanning the LG pump beam frequency with respect to an established resonant fundamental mode reference frequency, in a method similar to [26]. In this case, the configuration was as shown in figure 4. The cavity was locked to the fundamental mode of laser #2, and laser #1 was then phased-locked to laser #2. The error signal for the PLL was generated by sampling the fundamental mode beams from the lasers and detecting their beat on $PD_{\mathrm{PLL}}$. The PLL feedback acted on the frequency of laser #1 to fix the beat frequency equal to that of the local oscillator for the PLL. This local oscillator was scanned around a starting value of one FSR of the long cavity, to produce the required mode spectrum. As before, the critical alignment and mode-matching of the LG beam is assisted by pre-aligning the laser #1 with the mode generator bypassed.

## 4. Experimental results

We first present a comparison of the interferometric performance between higher-order LG modes and the fundamental mode beams. We continue with the results from the spectral analysis experiment involving astigmatism in the optical cavity, followed by other observations arising from our measurements involving mode mismatching and misalignment.

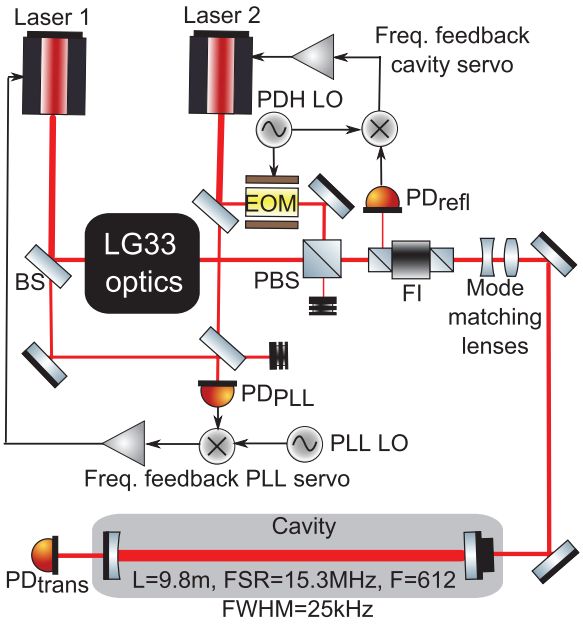


**Figure 4.** Experimental setup allowing detailed study of higher-order LG modes. Light from laser #2 is set resonant to the fundamental mode of the 9.8 m arm cavity by frequency feedback to the laser using the PDH method. The beam from laser #1 is phased-locked to laser #2, using a PLL, and then adjusted to the desired higher-order LG and injected into the arm cavity. By scanning the frequency of the PLL local oscillator the spectrum of the higher-order spatial modes excited by the LG beam can be determined. FI is a Faraday isolator, PDH LO and PLL LO are the local oscillators for the PDH cavity locking method and PLL, respectively.

### *4.1. Comparison of the interferometric performance between higher-order LG modes and the fundamental mode*

We compare the experimentally observed interferometric performance of an $LG_{3,3}$ beam and a fundamental mode beam in an environment similar to a full-scale GW detector. In order to make this comparison we examine the control signals generated in both cases. Apart from the type of beam our aim was to have the same conditions for the tests. As previously described, our procedure to set the alignment and mode matching of the optical cavity is by means of the fundamental mode beam transmitted through the LMC. When the $LG_{3,3}$ mode beam is chosen to be transmitted through the LMC, it should therefore already be aligned and mode matched without further adjustment.

In the top panels of figures 5 and 6, we show the resonance curve as observed in the light transmitted through the cavity in each case. The lower panels show the corresponding PDH error signals. Note that the zero cavity tuning was assigned to the peak of the dominant cavity resonance. A high speed video camera simultaneously recorded a sample of the cavity power in transmission which allowed us to identify the mode order resonant in the cavity when the $LG_{3,3}$ mode beam was injected. The insets in figure 6 show screenshots of the individual modes composing the resonance structure.

The frequency splitting arising with the $LG_{3,3}$ beam is clearly visible in the figure. The observed structure was repeatable across many FSRs and also over many days. The structure did not depend on the speed (within a range of one to a few FSRs per second) or direction of the sweep. Together these observations show that the structure originates from properties of the cavities, rather than the alignment at one time or another. As noted above, such a structure

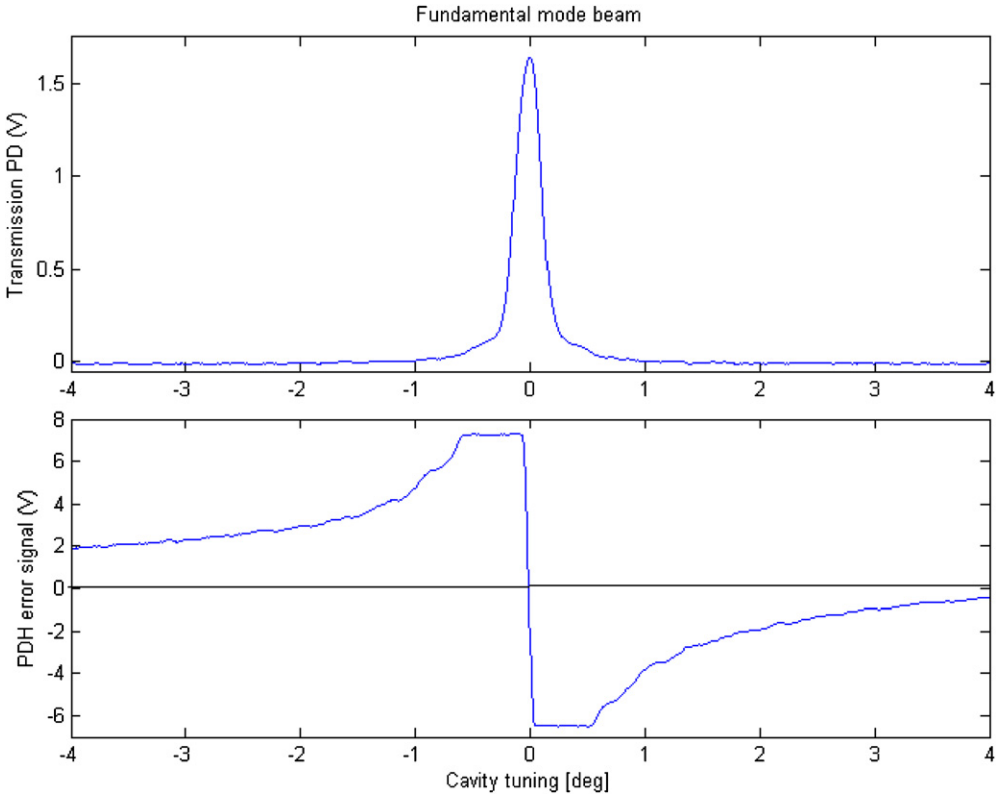


**Figure 5.** Dominant cavity resonance when the fundamental mode is injected (top). A single peak with the expected Lorentzian shape is observed. The associated PDH error signal presents saturation but otherwise it is as expected a single zero crossing.

of multiple peaks is expected in cavities with imperfect mirror surfaces, when operated with higher-order spatial modes. In such cases each of the peaks of the frequency splitting structure is associated with a pseudo-degenerate mode to the level of resolution determined by the cavity linewidth. This was confirmed by our high speed camera footage. The screenshots of the footage in figure 6 show several pseudo-degenerate HG shaped modes of order 7, and also a very faint $LG_{2,3}$ mode at the sides of the peak structure. The asymmetry of the peak structure is explained, in section 4.3, by small misalignments of the cavity.

The lower panels of figures 5 and 6 show that while the fundamental mode case presents a single high-gradient zero crossing, as desired, the $LG_{3,3}$ case presents multiple zero crossings. The reason for multiple zero crossings is the presence of pseudo-degenerate modes with frequency separation of the order of a cavity linewidth. PDH-based control systems usually operate at such a zero crossing, and the multiplicity of such arising from the pseudo-degenerate modes can therefore have two detrimental effects on the operation of a detector. First, the linear range of the error signal is considerably reduced making lock acquisition harder. Second, while it is possible to lock the cavity to a pseudo-degenerate mode, the stability of the lock would be degraded as undesired mode 'hopping' to nearby pseudo-degenerate modes may occur.

### *4.2. Effect of an astigmatic cavity*

The frequency splitting structure present on the cavity scans when an $LG_{3,3}$ mode beam was injected indicates the presence of surface distortions in the cavity mirrors. The starting point

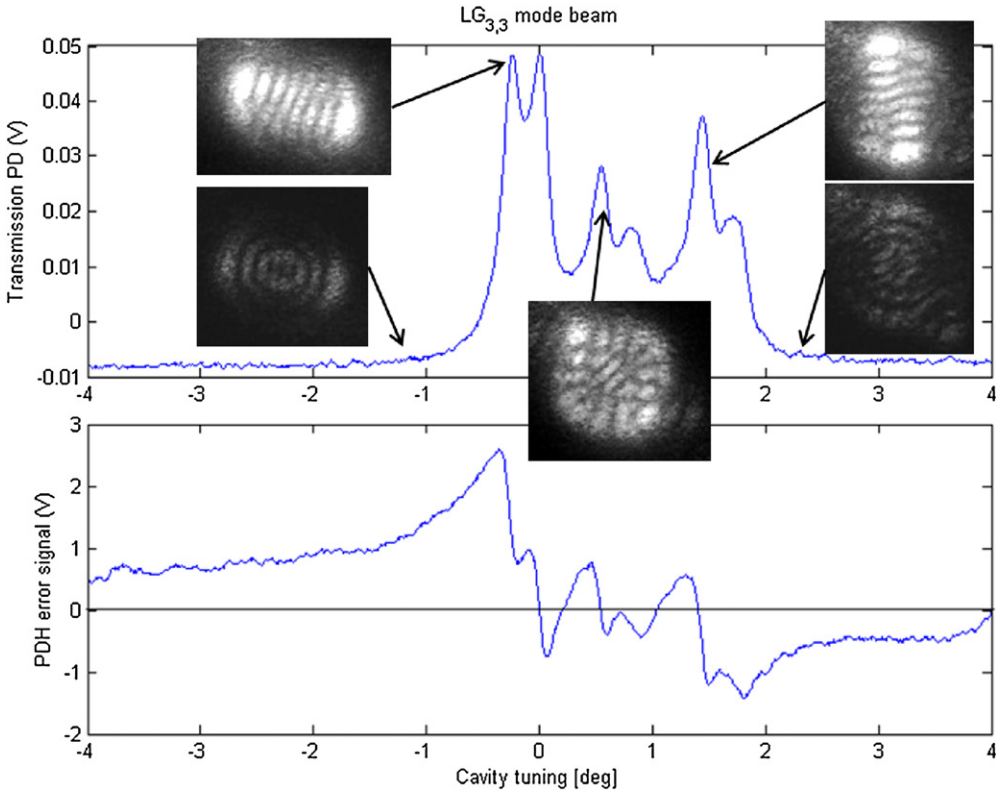


**Figure 6.** Dominant cavity resonance of order seven mode when the $LG_{3,3}$ mode is injected (top), explanation given in section 4.3. A multiple peak structure is observed where mode degeneracy was expected. The individual modes composing the resonance are clockwise from top right: HG-like$_{0,7}$, LG-like$_{2,3}$, HG-like$_{4,3}$, LG-like$_{2,3}$ and HG-like$_{7,0}$. The associated PDH error signal (bottom) presents multiple and nearby zero crossings which makes it difficult to stably lock the cavity to a specific pseudo-degenerate mode.

for our analysis of this effect is that astigmatism dominates the aberrations within the cavity. To understand this consider the inset video frames in figure 6. The three strongest pseudo-modes (brightest images) are each associated with a double-peak structure in the cavity scan. The remaining video frames show very faint $LG_{2,3}$ mode patterns found at the outer parts of the structure. It is notable that the observed modes are of order 7, even though an $LG_{3,3}$ beam is injected. The reason for this is described in section 4.3.

Here we consider other features that remained consistent during our experiments. First, the expected circularly symmetric modes were almost never observed, being replaced by those of rectangular (grid-like) pattern, as would be expected in the case that the cavity lacks cylindrical symmetry. This is supported by the relatively strong HG shaped modes seen in the video frames relative to the weak $LG_{2,3}$ mode. Second, the orientation of the HG shaped modes changes from the horizontally extended $HG_{7,0}$-like mode toward the left of the spectrum (as plotted), to the vertically extended $HG_{0,7}$-like mode towards the right. A similar astigmatic effect can be observed in the two slightly distorted $LG_{2,3}$ modes shown. In contrast the central double-peak feature is associated with an HG shaped mode that is extended about equally in the horizontal and vertical directions. This behavior is exactly what would be expected for an astigmatic cavity with the astigmatic axes aligned to the vertical and horizontal axes of the

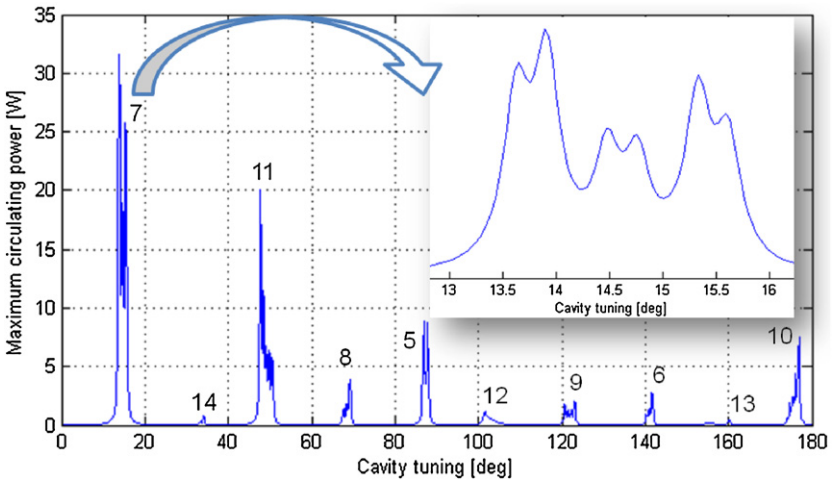


**Figure 7.** Finesse simulation of the Glasgow prototype cavity showing the mode coupling of the injected $LG_{3,3}$ mode beam while the cavity is scanned over a full FSR. The simulation included; a mode mismatch of 15% reduction in beam waist size and 1.5 m shift in its location, a misalignment of the ETM by 18 $\mu$rad in the vertical axis and an astigmatism of 5.25 cm longer horizontal $R_c$ of the ETM.

optical cavity, and such that the vertical radius of curvature is shorter than the horizontal one. Thus cavity modes that are spatially extended along the horizontal axis will see a cavity with a bigger g-factor, therefore smaller spatial mode spacing than cavity modes spatially extended along the vertical axis. This astigmatism also explains the observation that the cavity modes lack circular symmetry.

A simulation was performed using FINESSE software [27], to estimate the astigmatism of the ETM required to explain the observed level of frequency splitting. The results of the simulation are shown in figure 7. The simulation showed that the width of the spectral shape of the pseudo-degenerate mode structure was predominantly determined by the amount of astigmatism added (see the zoomed inset graph in figure 7). The effects of imperfect mode-matching and misalignment are discussed in section 4.3. Good agreement between model and experiment was obtained with an astigmatism, defined as $|R_{cy} - R_{cx}|$, of 5.25 cm (with the vertical radius of curvature shorter than the horizontal one).

To allow a detailed comparison of experiment with simulation, the PLL method (described above) was applied to yield an accurate, high resolution mode spectrum. A result is shown in figure 8. The stable operation provided in this mode allowed a CCD beam profiler to be employed to produce the detailed mode pictures shown in the figure (in this case of order 11).

High resolution scans were obtained for mode orders 5, 7, 9 and 11. The resulting spectra differed in fine-detail due to the size of the beams at the mirrors, indicating that the aberration is not purely astigmatic.

We use the round trip Gouy phase defined in equation 1 and the observed frequency spacing of the extreme HG-like modes in the various spectra to estimate the astigmatism of the ETM, as tabulated in table 1. This method assumes that the extreme HG-like modes, which are the most horizontally and vertically extended modes for each spectra, only observe the horizontal and vertical curvature of the mirrors respectively. This assumption is more accurate the higher the mode order. The astigmatism values given by the different mode orders scanned are consistent within their respective error range and consistent with our estimation of 5.25 cm (around 0.35% the ETM radius of curvature) derived from the FINESSE simulation.

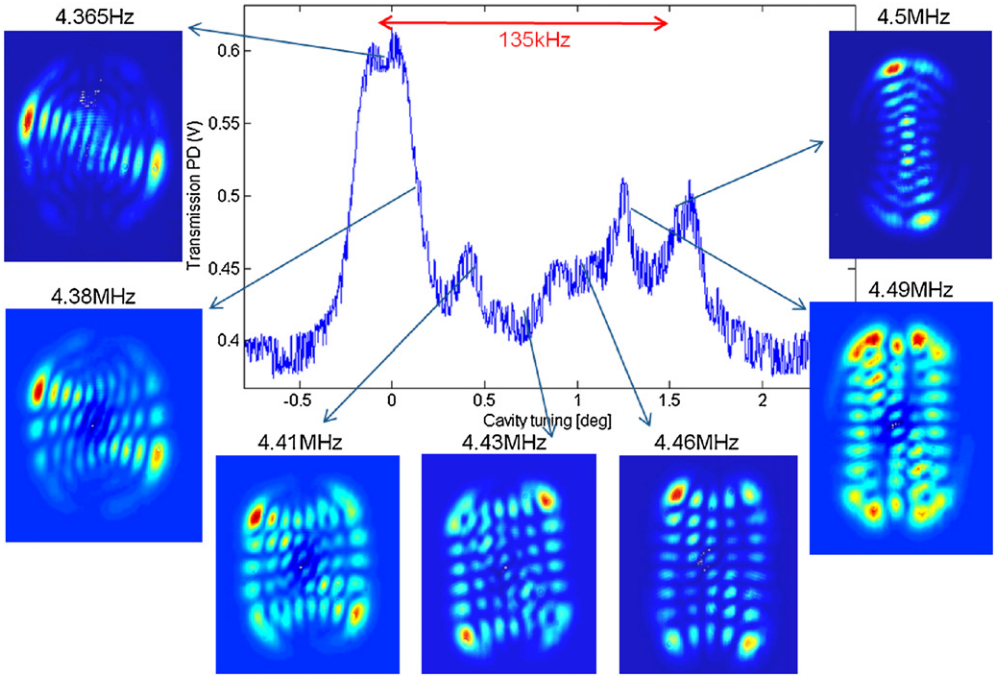


**Figure 8.** Intensity profile of the pseudo-degenerate HG shaped modes associated to the peaks of a frequency splitting structure of order 11. Clockwise from top right: HG-like$_{0,11}$ with LG-like mode, HG-like$_{2,9}$, HG-like$_{4,7}$, HG-like$_{6,5}$, HG-like$_{7,4}$, HG-like$_{9,2}$ with LG-like mode and HG-like$_{11,0}$ with LG-like mode.

**Table 1.** Experimental estimation of the ETM astigmatism by measuring the side frequencies (second and third columns) of the frequency splitting structures of the mode orders given in the first column. An error of 10 kHz was considered in the estimation of such frequencies from our experimental data. The fourth and fifth column shows the estimated radius of curvature and the sixth column shows associated astigmatism of the ETM.

| Mode Order | Freq. horizontal mode (MHz) | Freq. vertical mode (MHz) | ETM horizontal $R_c$ (m) | ETM vertical $R_c$ (m) | ETM astigmatism(cm) |
|---|---|---|---|---|---|
| 5 | $7.53 \pm 0.01$ | $7.61 \pm 0.01$ | $15.09 \pm 0.01$ | $15.02 \pm 0.01$ | $7 \pm 1$ |
| 7 | $1.39 \pm 0.01$ | $1.49 \pm 0.01$ | $15.081 \pm 0.007$ | $15.016 \pm 0.007$ | $6.4 \pm 0.7$ |
| 9 | $10.52 \pm 0.01$ | $10.65 \pm 0.01$ | $15.079 \pm 0.005$ | $15.014 \pm 0.005$ | $6.5 \pm 0.5$ |
| 11 | $4.37 \pm 0.01$ | $4.51 \pm 0.01$ | $15.079 \pm 0.004$ | $15.022 \pm 0.004$ | $5.7 \pm 0.4$ |

Attempts to measure the mirror figure on a Zygo phase shifting interferometer were hampered by interference from the rear-surface coating which was more reflective than the front surface at the 633 nm wavelength employed. Similarly a Wyko NT optical profiler failed to give consistent results for the large-scale curvature of the ETM, but did confirm that the mirror was locally smooth. This led us to consider more traditional techniques, namely the Ronchi and the Foucault methods, to determine the astigmatism.

The Ronchi method [28, 29] turns out to be best suited to systems with a small f-number (ratio of focal length to aperture), and in our application with a 15 m radius of curvature mirror of just a few cm aperture, the Foucault method proved more accurate, particularly as the astigmatism was by far the dominant aberration.

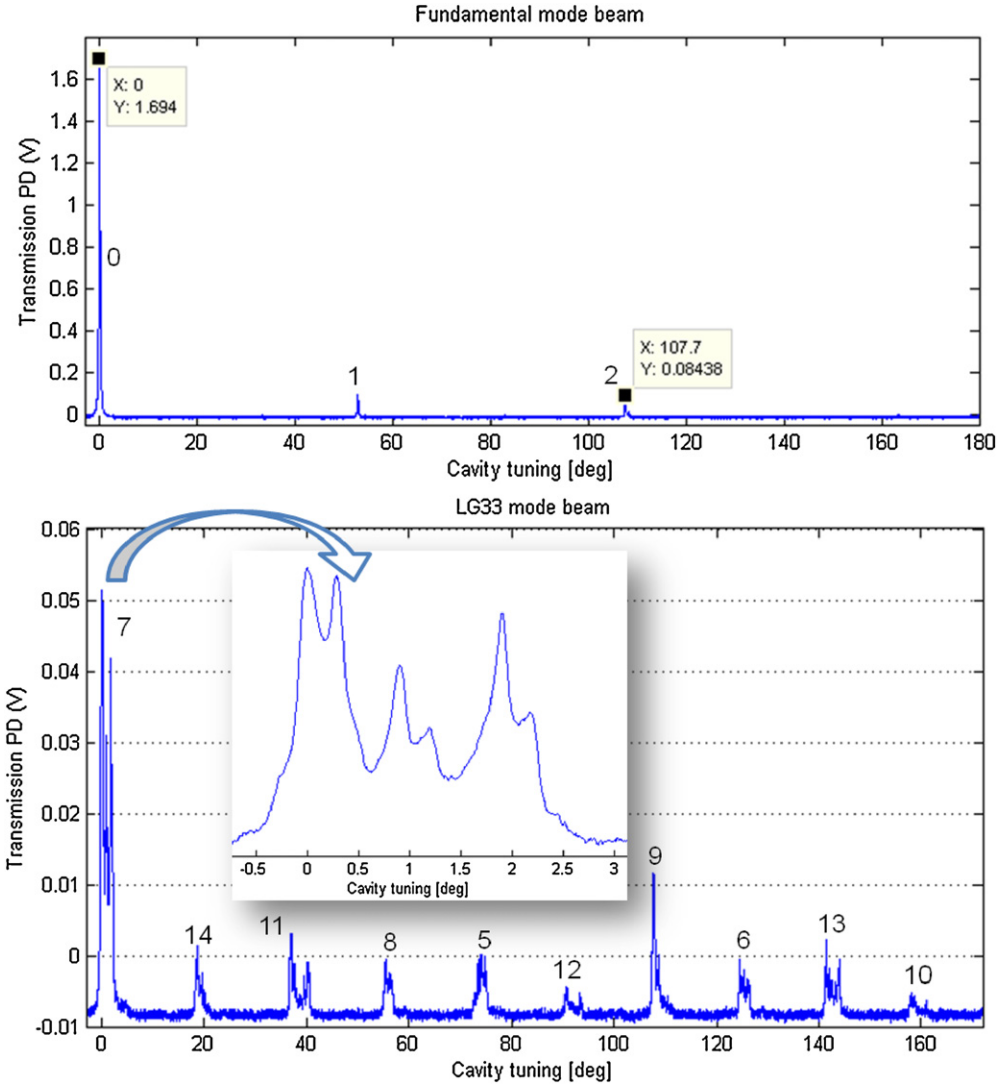


**Figure 9.** Measured cavity scans of our prototype's cavity for the same alignment and mode matching when the input beam was the fundamental mode (top) and the $LG_{3,3}$ mode (bottom) beams. The modes observed in the scan have been identified with their mode order.

In the Foucault test [30] a narrowband, diffuse, light source (in our case a green laser pointer fitted with a diffuser) is placed near the center of curvature (COC) of the mirror to be measured, such as to illuminate it, and the light reflected is directed back to form a focus close to the light source. A knife edge is moved across the beam, and the result of this is viewed (by eye or using a CCD video camera). On moving the knife an instant darkening of the mirror surface would be observed when the edge and the light source is at the COC. Otherwise we would observe the shadow of the sharp edge filling the mirror faster, the closer the sharp edge is to the COC. Thus the position of the focus is estimated.

As it involves a degree of judgement, we conducted several mutually blind trials of this method, and obtained results consistent within our stated error estimate. The measurement was repeated with the mirror rotated 90 degrees and the astigmatism obtained in this way was

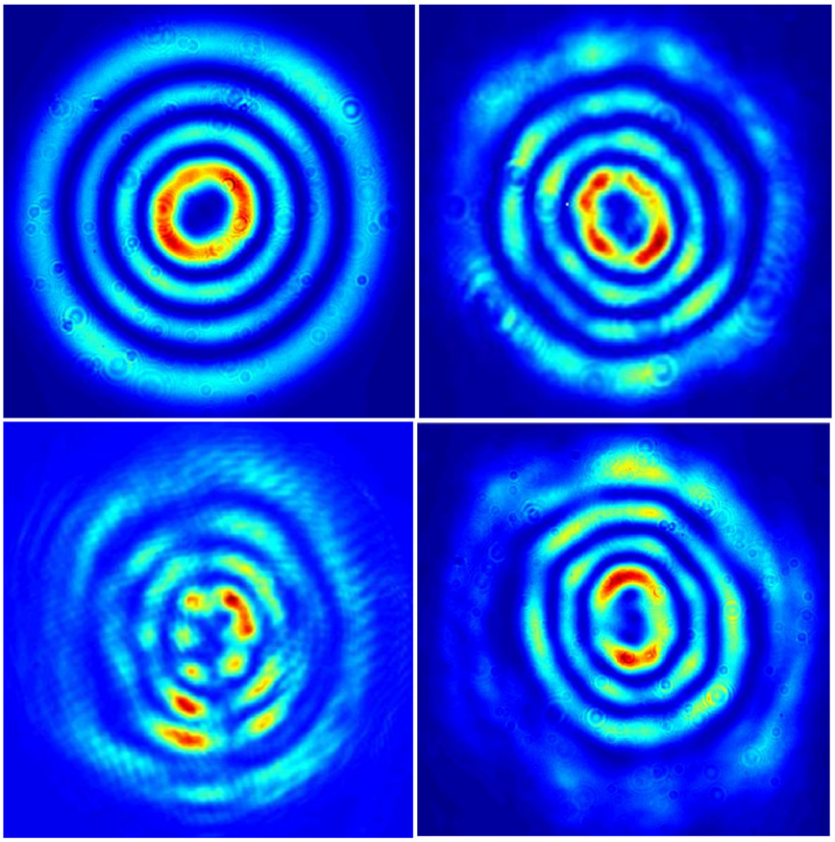

**Figure 10.** Degradation of the $LG_{3,3}$ beam at different points of the Glasgow prototype. Clockwise from top left: the beam with highest $LG_{3,3}$ purity content immediately after the LMC, the beam after passing through EOM crystals and a FI, the beam just before the ITM and the beam transmitted by the ETM with the cavity misaligned. For the last two images a lens was used to focus the beam to within the profiler's CCD active area. Intensity profiles are normalized in all cases.

$5.3 \pm 0.5$ cm, with the horizontal radius of curvature of the mirror being longer than the vertical one. This result agrees with our previous observations and with the astigmatism values given in table 1.

### *4.3. Effect of mode-mismatch and cavity misalignment*

In figure 6 we observe that modes of order 7 were dominant even when the illuminating beam was $LG_{3,3}$. The effect is also clear in figure 9 where the mode spectra resulting from fundamental and $LG_{3,3}$ input beams are compared. Note that in the former case the power ratio from order 0 to orders 1 or 2 is 21:1, while the latter case is more complicated.

The presence of so many different higher-order spatial modes can be partly attributed to the degradation in the purity of the injected $LG_{3,3}$ beam. Figure 10 shows the degradation of the intensity profile of the $LG_{3,3}$ beam from its highest purity just after the LMC (top left) as it passes through several transmissive optics in the input bench (after EOM crystals and an FI, top right), also just before the 10 m cavity input mirror (ITM), to the lowest purity point at the cavity end mirror transmission, measured with the cavity misaligned (the light power here was much lower than in the other cases and close to the profiler limit). A pure $LG_{3,3}$ mode

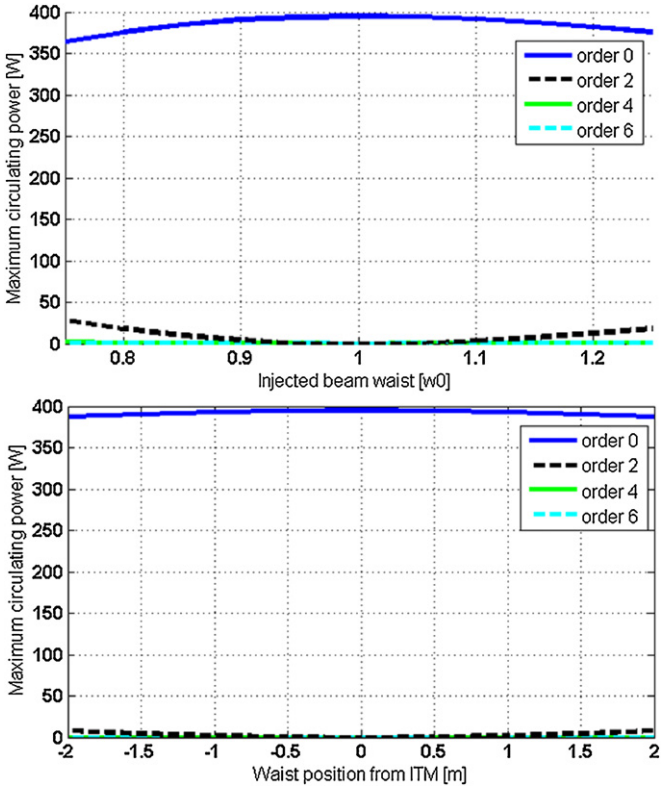


**Figure 11.** Simulation of mode coupling, with a fundamental mode input beam, due to a mode mismatch resulted from; beam waist size difference respect to the cavity waist $w_0$ (top), and position of the beam waist away from the ITM (bottom).

was fitted and removed to each measured profile, resulting in maximum normalized residuals of 0.12, 0.33, 0.39 and 0.5, respectively.

The observed degradation of the $LG_{3,3}$ beam through the system is due to its wider intensity profile in comparison with the fundamental mode beam, for which the system was originally designed. Although we checked that all clear apertures were adequate, some were only just so. Even though the resulting beam distortions affect the mode scans at some level, they cannot explain major features, in particular why mode orders 7 and 11 were dominant when order 9 was injected.

The FINESSE model was employed to simulate the relationship between mode-matching errors and mode coupling. In our cavity, in which the ITM is plane, mode matching errors can arise due to incorrect positioning of the waist of the incoming beam (the waist should be at the ITM) and/or incorrect sizing of that waist.

We started simulating in FINESSE the fundamental mode, used to match and pre-align the cavity. The best fit to experimental data requires that we have a 15% smaller waist positioned 1.5 m from the ITM to obtain the observed ratio of fundamental mode to the mode of order 2. Beam-profile measurements of our experimental mode matching show comparable levels of mode mismatch. The relationships between these errors and the mode matching are illustrated in figure 11. In the $LG_{3,3}$ case the results are shown in figure 12. This simulation shows that injecting a beam waist 0.85 or 1.18 times the cavity waist leads to considerable coupling into mode orders 7 and 11, as observed experimentally. To achieve this with an incorrectly located

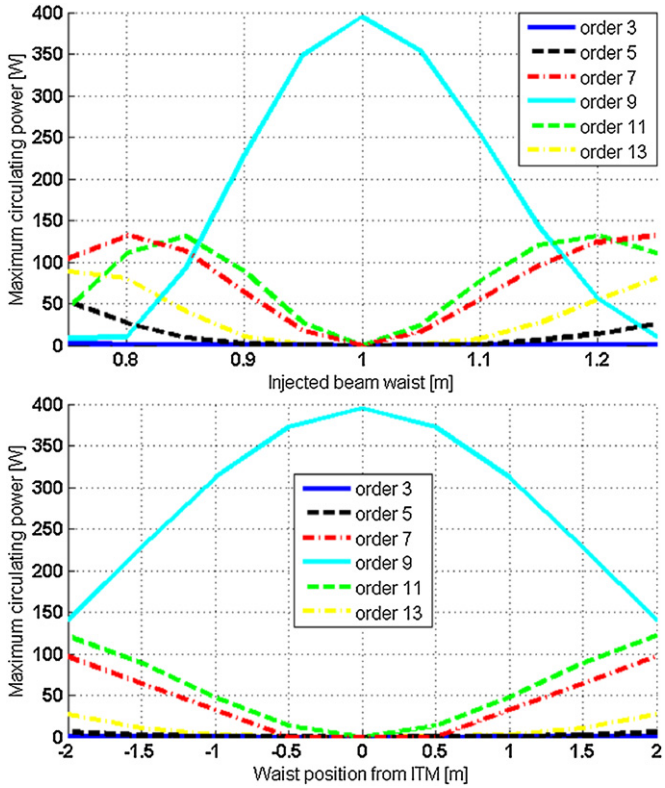


**Figure 12.** Simulation of mode coupling in our cavity (for mode orders 1 to 13), with an input mode order 9, due to a mode mismatch resulted from; beam waist size difference respect to the cavity waist $w_0 = 1.548$ mm (top), and position of the beam waist away from the ITM (bottom).

waist would indicate an error of more than 2 m. Although the mode mismatch is likely to have been a mixture of the two effects, waist size deviation was probably the dominant factor in our case.

When we combine both sources of mode mismatch (at the previously estimated levels) in the simulations for the $LG_{3,3}$ input beam, we observe that order 7 becomes the dominant mode, followed by order 11 and then order 9. This closely matches our observations, although in the experimental scan at the bottom of figure 9 we see order 11 being weaker than 9. This is explained by the wider intensity pattern of order 11 suffering from clipping on the cavity input mirror.

Comparing figures 12 and 11 shows that the coupling into higher-order modes is much weaker for the fundamental mode compared to the $LG_{3,3}$ mode, for a given matching error. This fits with our experience in conducting the experiment.

During our experiments we also noticed that contrary to our assumption, the beam properties of the LMC transmitted fundamental mode and $LG_{3,3}$ mode beams were different. We measured and compared the beam radius and location immediately after the LMC. Figure 13 shows an accurate fitting of the measurements of both beams to a Gaussian beam radius profile. The fundamental mode beam presents two sets of data corresponding to the vertical and horizontal output of the beam profiler. The horizontal data fitted the Gaussian beam profile much better. On the other hand the beam radius of the $LG_{3,3}$ mode beam was obtained by fitting a pure helical $LG_{3,3}$ mode intensity profile to the recorded intensity profiles. This

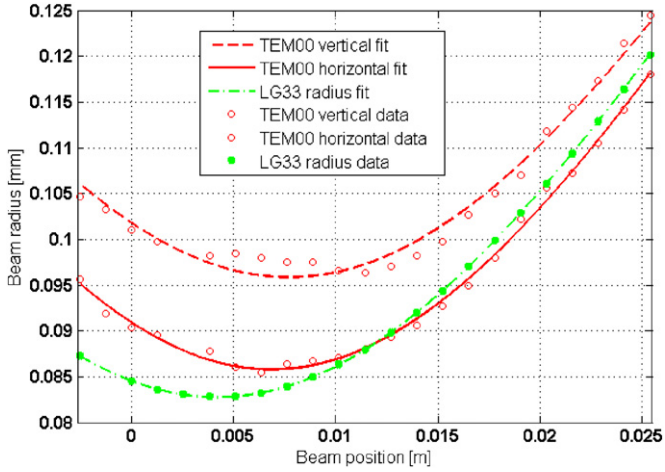


**Figure 13.** Beam size radius and position, measured after the LMC, for the fundamental mode beam (data points shown as circles and fitted to a Gaussian beam profile shown in red dark color lines) and the $LG_{3,3}$ mode beam (data points shown as stars and fit shown in green light color line). The beam waist size is given by the minimum point of the fitted curves. Notice that the fundamental mode shows both the horizontal and the vertical beam radius.

figure clearly shows a disagreement in both the beam waist position and size (of 3.3 mm and 3.7% respectively). The different beam parameters of the fundamental and the $LG_{3,3}$ modes after the LMC indicate that the effective mirror surface profiles of the LMC mirrors must have been different for the two different mode patterns and lateral extents. This effect is likely to have contributed significantly to the mode-mismatch observed for the $LG_{3,3}$ beam.

We conclude this section by referring to the asymmetry observed on the structure of the pseudo-degenerate modes, where the peaks associated with the modes spatially extended along the horizontal axis contain more power than those extended along the vertical axis. This is shown in the frequency splitting structure of figures 6 and 8. We again used numerical simulations and altered the cavity alignment values, with a fundamental mode input beam, until we obtained similar power relations between the cavity modes order 0, 1 and 2 shown on top of figure 9. This corresponded to a misalignment of 18 $\mu$rad. If the misalignment was applied about the cavity vertical axis then the simulations (see figure 7) showed a similar asymmetry to that seen in figure 6 where the peaks associated with the modes spatially extended through the horizontal axis were dominant.

## 5. Conclusions

The aim of our work was to gain practical experience in coupling higher-order LG modes to a cavity typical of those employed in ground based gravitational wave detectors. This has led to improved understanding of the design requirements applicable to future full-length interferometers.

Our quantitative conclusions are presented in two parts: first we consider the mode-matching errors that are tolerable when $LG_{3,3}$ beams are employed, then we evaluate the tolerance of such a system to astigmatism of the mirror surfaces.

Although mode-matching is usually considered to be a matter of basic design, it is clear that our approach of pre-matching to the fundamental mode and later switching to the desired higher-order mode that has been passed through the same filter cavity, did not work as well

as expected. Indeed in our experiment we did not obtain a stable, efficiently-coupled $LG_{3,3}$ mode, and the matching was much better for the seventh order LG modes.

With the fundamental mode the ratio of the fundamental to the next dominant mode (order 2) power coupled to the cavity was 21:1. The simulation results show that for a non astigmatic cavity with the same properties as the Glasgow prototype and perfectly aligned, in order to get the same level of power relation when the input beam is an $LG_{3,3}$ mode we would require a mode matching of the beam waist size no worse than 4.6%, assuming the beam waist is perfectly located at the ITM. If we allow for some error in the beam waist location of around 0.5 m then the beam waist size error should be smaller than 3%.

In a full-scale detector, acceptable matching errors are likely in the region of 1%. Applying this target to the cavity geometry of our experiment yields a maximum allowable beam waist size error, assuming the waist is correctly located, of 1.1%, or, for a correctly sized waist, a maximum position error of 0.22 m. These are 8 and 6.5 times smaller errors, respectively, than would be tolerable in the fundamental mode case, for the same matching error.

With respect to astigmatism, at the start of the experiment we had no indication that the figure of ETM, in particular, would be other than a well-figured spherical mirror. It became clear, however, that the astigmatism was enough to break the degeneracy of the various nominally degenerate LG modes. The resulting pseudo-degenerate modes share the optical power that would exist in the cavity if they were degenerate. Thus when locking the cavity to one of the pseudo-degenerate modes the intracavity power would be considerably smaller than expected in the ideal spherical-mirror case.

Once again, in a full-scale detector acceptable errors are likely to be set at no more than 1%. Our simulations show that in a perfectly aligned and mode matched cavity the tolerable astigmatism would be less than 1.9 mm on a 15 m ETM, or equivalently an astigmatism of 0.012% the ETM radius of curvature, assuming that the ITM is non astigmatic. An analysis of the mode coupling due to astigmatism on longer cavities with larger mirrors, i.e. aLIGO style arm cavities, can be found in [20].

To facilitate bonding of fittings required for their suspension [31] mirrors of a gravitational wave detector are frequently shaped, as was our ETM, with diametrically opposing vertical flat faces polished ground into the cylindrical barrel surface. We observed that both the mode structure and the ETM astigmatism were aligned to horizontal-vertical axes. The surface profiles of the non-coated substrate of the ETM do not show such levels of astigmatism. Therefore we suspect that the astigmatism originates from coating stress introduced during the ion-beam sputtering process, as described in [32], which is carried out at some elevated temperature (the details of the proprietary process are unknown to us). When the mirror is finally cooled a radially asymmetrical stress field arises due to the non radial symmetry of the substrate.

In the generation of the $LG_{3,3}$ mode it is also important to consider that if the mode matching is done through the fundamental mode transmitted by the LMC (as in our work) then the LMC cavity mirrors need to be of better quality than the ones we used so that the mode matching of the fundamental and $LG_{3,3}$ beams are consistent. Notice that the cavity mirrors in the used LMC were clamped instead of glued which might have influenced the quality of the current mirrors.

The enhancements required to enable the application of higher-order LG modes in gravitational wave detectors are matters of improved design and fabrication of optical components, and as such are likely to be amenable to solution through refinement of existing processes.

Finally we note that the work presented in this paper is also relevant to neighboring fields, such as quantum optics and atom trapping [33].

## Acknowledgments

The authors are grateful for the support from the University of Glasgow and the University of Birmingham and from the Science and Technologies Facility Council (STFC).

## References

[1] Harry G M *et al* 2010 Advanced LIGO: the next generation of gravitational wave detectors *Class. Quantum Grav.* **27** 084006
[2] (The Virgo Collaboration) 2009 Advanced Virgo baseline design *Technical Report* VIR-027A-09
[3] Abbott B *et al* 2009 LIGO: the laser interferometer gravitational-wave observatory *Rep. Prog. Phys.* **72** 076901
[4] Accadia T *et al* 2012 Virgo: a laser interferometer to detect gravitational waves *J. Instrum.* **7** P03012
[5] Abadie J *et al* 2010 Predictions for the rates of compact binary coalescences observable by ground-based gravitational-wave detectors *Class. Quantum Grav.* **27** 173001
[6] Penn S D *et al* 2003 Mechanical loss in tantala/silica dielectric mirror coatings *Class. Quantum Grav.* **20** 29172928
[7] DeSalvo R 2002 Path-finding towards a cryogenic interferometer for LIGO *Class. Quantum Grav.* **19** 2021
[8] Martin I W *et al* 2011 Low loss coatings for future gravitational wave detectors *Amaldi 9* (Cardiff, UK)
[9] Mours B, Tournefier E and Vinet J-Y 2006 Thermal noise reduction in interferometric gravitational wave antennas: using high order TEM modes *Class. Quantum Grav.* **23** 5777
[10] Vinet J-Y 2009 On special optical modes and thermal issues in advanced gravitational wave interferometric detectors *Living Rev. Rel.* **12** 5 www.livingreviews.org/lrr-2009-5
[11] Tarallo M G *et al* 2007 Generation of a flat-top laser beam for gravitational wave detectors by means of a nonspherical Fabry–Perot resonator *Appl. Opt.* **46** 6648–54
[12] Bondarescu M, Kogan O and Chen Y 2008 Optimal light beams and mirror shapes for future LIGO interferometers *Phys. Rev.* D **78** 082002
[13] Chelkowski S, Hild S and Freise A 2009 Prospects of higher-order Laguerre–Gauss modes in future gravitational wave detectors *Phys. Rev.* D **79** 122002
[14] Kennedy S A, Szabo M J, Teslow H, Porterfield J Z and Abraham E R I 2002 Creation of Laguerre–Gaussian laser modes using diffractive optics *Phys. Rev.* A **66** 043801
[15] Fulda P, Kokeyama K, Chelkowski S and Freise A 2010 Experimental demonstration of higher-order Laguerre–Gauss mode interferometry *Phys. Rev.* D **82** 012002
[16] Punturo M *et al* The third generation of gravitational wave observatories and their science reach *Class. Quantum Grav.* **27** 084007
[17] Hild S *et al* 2011 Sensitivity studies for third-generation gravitational wave observatories *Class. Quantum Grav.* **28** 094013
[18] Drever R W P, Hall J L, Kowalski F V, Hough J, Ford G M, Munley A J and Ward H 1983 Laser phase and frequency stabilization using an optical resonator *Appl. Phys.* B **31** 97–105
[19] Siegman A E 1986 *Lasers* (Sausalito, CA: University Science Books)
[20] Bond C, Fulda P, Carbone L, Kokeyama K and Freise A 2011 Higher order Laguerre–Gauss mode degeneracy in realistic, high finesse cavities *Phys. Rev.* D **84** 102002
[21] Hong T, Miller J, Yamamoto H, Chen Y and Adhikari R 2011 Effects of mirror aberrations on Laguerre–Gaussian beams in interferometric gravitational-wave detectors *Phys. Rev.* D **84** 102001
[22] Huttner S H, Barr B W, Plissi M, Taylor J, Sorazu B and Strain K A 2007 Novel sensing and control schemes for a three-mirror coupled cavity *Class. Quantum Grav.* **24** 3825
[23] Edgar M *et al* 2010 Experimental demonstration of a suspended, diffractively coupled Fabry-Perot cavity *Class. Quantum Grav.* **27** 084029
[24] Friedrich D *et al* 2011 Waveguide grating mirror in a fully suspended 10 meter Fabry–Perot cavity *Opt. Express* **19** 14955–63
[25] Willke B *et al* 2002 The GEO 600 gravitational wave detector *Class. Quantum Grav.* **19** 1377
[26] Stochino A, Arai K and Adhikari R X 2012 Technique for in-situ measurement of free spectral range and transverse mode spacing of optical cavities *Appl. Opt.* **51** 6571
[27] Freise A, Heinzel G, Lueck H, Schilling R, Willke B and Danzmann K 2004 Frequency-domain interferometer simulation with higher-order spatial modes *Class. Quantum Grav.* **21** S1067–74
[28] Anderson J A and Porter R W 1929 Ronchi's method of optical testing *Astrophys. J.* **70** 175
[29] Mansuripur M 1997 The Ronchi test *Opt. Photon. News* **8** 42–6
[30] http://atm-workshop.com/foucault.html

[31] Cumming A V *et al* 2012 Design and development of the advanced LIGO monolithic fused silica suspension *Class. Quantum Grav.* **29** 035003
[32] Srinivasan K 1977 Coating strain induced distortion in LIGO optics LIGO-T970176-00 https://dcc.ligo.org/public/0028/T970176/000/T970176-00.pdf
[33] Franke-Arnold S, Allen L and Padgett M 2008 Advances in optical angular momentum *Laser Photon. Rev.* **2** 299–313